Vol. 6, No. 1, February 2022, pp. 1-9

Current Optics and Photonics

Regular Paper

# Improved Iterative Method for Wavefront Reconstruction from Derivatives in Grid Geometry

**Vu-Hai-Linh Nguyen[1,2], Hyug-Gyo Rhee[1,2]*, and Young-Sik Ghim[1,2]****

[1]*Department of Science of measurement, University of Science and Technology, Daejeon 34113, Korea*
[2]*Optical Imaging and Metrology Team, Advanced Instrumentation Institute, Korea Research Institute of Standards and Science, Daejeon 34113, Korea*

(Received September 3, 2021 : revised October 15, 2021 : accepted November 2, 2021)

This paper proposes a robust, simple zonal wavefront-estimation method in a grid sampling model. More slopes are added to the integral equation of the algorithm to improve the accuracy and convergence rate of this approach, especially for higher-order optical aberrations. The Taylor theorem is applied to clarify the mathematical description of the remaining error in the proposed method. Several numerical simulations are conducted to ensure the performance and improvement in comparison to the Southwell and previous algorithm. An experiment is also conducted according to deflectometry output and the results are verified using a reference measured with a stylus system.

*Keywords* : Deflectometry, Shack-Hartmann sensor, Slopes measurement, Wavefront reconstruction
*OCIS codes* : (010.7350) Wave-front sensing; (120.5050) Phase measurement

## I. INTRODUCTION

Along with the evolution of adaptive optics (AO) and surface-measurement methods over the last few decades, the need for wavefront measuring methods is now seen. For instant, the Shack-Hartmann wavefront sensor is widely utilized to investigate wavefront aberrations in many AO applications [1–3], owing to its simple setup and operation, while lateral shearing interferometry and deflectometry are bright candidates for optical-based three-dimentional (3D) shape measuring due to their reference-free approaches [4, 5]. One factor in common in those systems is their output: local wavefront slopes. Thus, there is rising demand for phase retrieval techniques derived from gradient data.

Phase and surface profile reconstruction problems were initially investigated in 1974 by Rimmer [6]. Later, various wavefront reconstruction techniques were introduced [7–10]. They can be grouped into modal and zonal methods [11]. The former use certain special sets of polynomials, such as the Zernike polynomial, to fit the wavefront aberration or slopes [12]. On the other hand, zonal approaches use a grid configuration to describe the relation between heights and slopes, and then estimate height from slope based on an iterative or least-squares method. There are three basic discrete geometries capable of converting measured slopes to the phase profile, as addressed by Southwell [11], Hudgin [13] and Fried [14]. Among them, Southwell's algorithm is considered to be the most efficient, due to its simple formula and associated error propagation [15] and its suitability for several types of sensors. In this geometry, an integral equation is formed to associate the unknown wavefront points with the corresponding gradient in the horizontal as well as the vertical direction, after which the set of relationship equations is solved to obtain the phase values. The classic Southwell algorithm yields good results when used to reconstruct every combination of lower order optical aberrations, such as tilt, astigmatism, defocus, and coma. When the wavefront is of a higher order, this method

*Corresponding author: hrhee@kriss.re.kr, ORCID 0000-0003-3614-5909
**Corresponding author: young.ghim@kriss.re.kr, ORCID 0000-0002-4052-4939

Color versions of one or more of the figures in this paper are available online.



pISSN: 2508-7266 / eISSN: 2508-7274 https://doi.org/10.3807/COPP.2022.6.1.001

has limitations [9]. In recent work, Li *et al*. [16] proposed an algorithm to improve the truncation error in Southwell's geometry by increasing the quantity of slopes in the estimated phase equation. However, Li's approach uses only slopes in the vertical and horizontal directions. In other papers, Pathak and Boruah [17] and Phuc *et al*. [18] utilized diagonal phases and slopes to gain a greater number of gradients. This method remains limited due to the increasing separation between the diagonal grid point and the center phase points.

In this study, we propose a new approach to incorporate more slopes in the integral equation, to reduce the algorithmic error of wavefronts consisting of higher-order aberrations. The second advantage of the proposed method is its considerable improvement of the convergence rate of an iterative solution, and hence the lack of a need for a trade-off between algorithm speed and accuracy. The remainder of this paper is as follows. It begins by providing a brief description of the traditional Southwell algorithm, and a theoretical description of our own algorithm. The mathematical expression of the algorithmic error in our approach is also derived and analyzed in section II, to prove its efficiency when used to reconstruct higher-order aberrations. The results of numerical simulations to verify the accuracy, convergence rate, and noise sensitivity are given in section III. In section IV we apply the proposed algorithm in an experiment to output the defelectometry, and compare to the results of a commercial stylus system to ensure the algorithm's validity. Finally, the work is discussed and concluded in section V.

## II. PROPOSED ALGORITHM MODEL AND DESCRIPTION OF ITS REMAINING ERRORS

### 2.1. Algorithm Operation

It is assumed that the wavefront can be described with the grid geometry in Fig. 1. To reconstruct the center phase point, Southwell's algorithm [11] derives an integration equation from data of four surrounding points in the horizontal and vertical directions:

$$\frac{W - W_4}{h} = \frac{S_x + S_{4x}}{2}, \tag{1}$$

$$\frac{W_5 - W}{h} = \frac{S_{5x} + S_x}{2}, \tag{2}$$

$$\frac{W - W_2}{h} = \frac{S_y + S_{2y}}{2}, \tag{3}$$

$$\frac{W_7 - W}{h} = \frac{S_{7y} + S_y}{2}. \tag{4}$$

Here, $W$ and $S$ are the wavefront phase points and slopes, respectively and $h$ is the gap between two phase points.

Therefore, the center phase point can be described as follows:

$$W = \frac{W_4+W_5+W_2+W_7}{4} + \frac{h}{8} \times (S_{4x} - S_{5x} + S_{2y} - S_{7y}). \tag{5}$$

To increase the number of slopes in the integration equation, Pathak introduces a modified algorithm that uses four additional points and corresponding gradients, in the corners [17, 18]. The formula for estimating the wavefront phase value is given as follows:

$$W = \frac{1}{8}\sum_{i=1}^{8} W_i + \frac{h}{16} \times (S_{4x} - S_{5x} + S_{2y} - S_{7y} - S_{8x} - S_{8y} + S_{1x} + S_{1y} - S_{3x} + S_{3y} + S_{6x} - S_{6y}). \tag{6}$$

To incorporate more gradients in the phase equation without using corner phase points, our approach separates the nine grid points in Fig. 1 into four domains, as shown in Fig. 2.

We now apply the Southwell integral equation to the four points in each domain. For instance, in domain 1 the following applies:

$$\frac{W_2 - W_1}{h} = \frac{S_{2x} + S_{1x}}{2}, \tag{7}$$

$$\frac{W - W_4}{h} = \frac{S_x + S_{4x}}{2}, \tag{8}$$

$$\frac{W_4 - W_1}{h} = \frac{S_{4y} + S_{1y}}{2}, \tag{9}$$

$$\frac{W - W_2}{h} = \frac{S_y + S_{2y}}{2}. \tag{10}$$

Combining Eqs. (7)–(10), we have

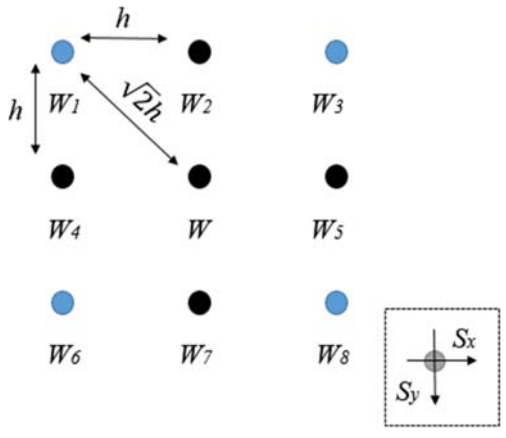


**FIG. 1.** Grid sampling geometry for the zonal wavefront-reconstruction method. In this geometry, the phase values coincide with the vertical and horizontal slopes at each grid point.

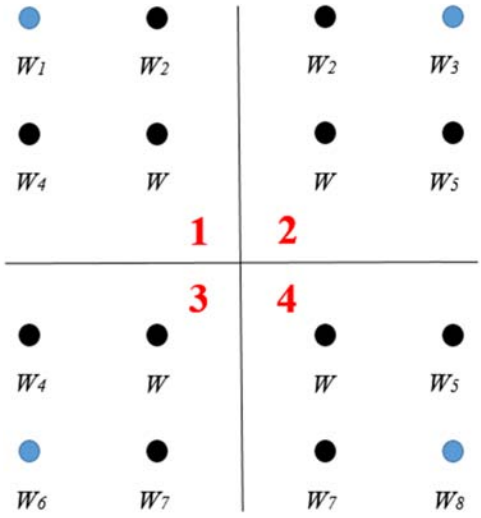


**FIG. 2.** Domain divided: each set of nine grid points is sorted into four groups. There are four phase points in each group.

$$W = W_1 + \frac{h}{4} \times (S_x + S_{1x} + S_{2x} + S_{4x} + S_y + S_{1y} + S_{2y} + S_{4y}). \quad (11)$$

Equation (11) represents the relationship between the estimated phase point $W$ and all slopes in domain 1. For the other domains, the equation can be formulated as

$$W = W_3 + \frac{h}{4} \times (-S_x - S_{2x} - S_{3x} - S_{5x} + S_y + S_{2y} + S_{3y} + S_{5y}), \quad (12)$$

$$W = W_6 + \frac{h}{4} \times (S_x + S_{4x} + S_{6x} + S_{7x} - S_y - S_{4y} - S_{6y} - S_{7y}), \quad (13)$$

$$W = W_8 + \frac{h}{4} \times (-S_x - S_{5x} - S_{7x} - S_{8x} - S_y - S_{5y} - S_{7y} - S_{8y}). \quad (14)$$

By adding the four equations above, we have

$$W = \frac{W_1 + W_3 + W_6 + W_8}{4} + \frac{h}{16} \times (2S_{4x} - 2S_{5x} + 2S_{2y} - 2S_{7y} - S_{8x} - S_{8y} + S_{1x} + S_{1y} - S_{3x} + S_{3y} + S_{6x} - S_{6y}). \quad (15)$$

Equation (15) provides the estimated phase equation with four surrounding points with the number of slopes increased to 12. The equation for the algorithm's remaining error is a function of the distance $h$ between two phase points in grid. This error increases as $h$ increases. Therefore, the advantages of our integral equation are that we indirectly add the slopes in Eq. (15) by divided the grid into subdomains, instead of directly using the relation of center phase and corner phase, where the distance becomes $\sqrt{2}h$. In addition, in the estimated phase equation the phase points are variables. By reducing the number of variables in our proposed system of linear equations in Eq. (15) to 4, the system will have more zero elements and will be easier to solve.

In this investigation, to ensure the best performance we use an iterative method called the successive over-relaxation (SOR) [19] technique to solve Eq. (15). If the form of the equation is

$$x_{n+1} = f(x_n), \quad (16)$$

the SOR solution then becomes

$$x_{n+1}^{\mathrm{SOR}} = (1 - \omega)x_n^{\mathrm{SOR}} + \omega f(x_n^{\mathrm{SOR}}), \quad (17)$$

where $\omega$ is the optimal relaxation factor:

$$\omega = \frac{2}{1 + \sin[\pi/(N+1)]}. \quad (18)$$

### 2.2. Mathematical Description of the Error of the Algorithm

In this section, we evaluate the error of the algorithm using the approximate calculation of Eq. (15). We begin with the expression of the Taylor theorem [20]. This theorem states that any continuous function $f(x)$ that has derivatives $f'(x) \ldots f^n(x)$ within interval $[x_o, x]$ can be represented by the following series:

$$f(x) = f(x_0) + (x - x_0)f'(x_0) + (x - x_0)^2 \frac{f''(x_0)}{2!} + \cdots. \quad (19)$$

In the grid model with spacing $h$ shown in Fig. 1, Eq. (16) can be rewritten as follows:

$$f(x) = f(x_0) + hf'(x_0) + h^2 \frac{f''(x_0)}{2!} + \cdots. \quad (20)$$

We now apply the Taylor theorem to every phase point of the grid geometry. For example, for the first domain in Fig. 2, we have the following:

$$W = W_2 + hS_{2y} + \frac{h^2}{2}S'_{2y} + \frac{h^3}{3!}S''_{2y} + \cdots, \quad (21)$$

$$W = W_4 + hS_{4x} + \frac{h^2}{2}S'_{4x} + \frac{h^3}{3!}S''_{4x} + \cdots, \quad (22)$$

$$W_1 = W_2 - hS_{2x} + \frac{h^2}{2}S'_{2x} - \frac{h^3}{3!}S''_{2x} + \cdots, \quad (23)$$

$$W_1 = W_4 - hS_{4y} + \frac{h^2}{2}S'_{4y} - \frac{h^3}{3!}S''_{4y} + \cdots. \quad (24)$$

Combining Eqs. (21) and (24) gives

$$2(W - W_1) = h(S_{2x} + S_{2y} + S_{4x} + S_{4y}) + \frac{h^2}{2}(S'_{2y} + S'_{4x} - S'_{2x} - S'_{4y}) + \cdots. \quad (25)$$

Similarly, the relationship expressions for the three other domains in Fig. 2 can be written as

$$2(W - W_3) = h(S_{2y} - S_{2x} + S_{5y} - S_{5x}) + \frac{h^2}{2}(S'_{2y} + S'_{5x} - S'_{2x} - S'_{5y}) + \cdots, \quad (26)$$

$$2(W-W_6)=h(S_{4x}-S_{7y}-S_{4y}+S_{7x})+\frac{h^2}{2}(S'_{7y}+S'_{4x}-S'_{7x}-S'_{4y})+\cdots, \quad (27)$$

$$2(W-W_8)=h(-S_{5x}-S_{7y}-S_{7x}-S_{5y})+\frac{h^2}{2}(S'_{7y}+S'_{5x}-S'_{7x}-S'_{5y})+\cdots. \quad (28)$$

From Eqs. (25)–(28), we can further obtain

$$\begin{aligned}8W=&\,2(W_1+W_3+W_6+W_8)+2h(S_{4x}-S_{5x}+S_{2y}-S_{7y})\\&+h^2(S'_{4x}+S'_{5x}+S'_{2y}+S'_{7y}-S'_{2x}-S'_{4y}-S'_{7x}-S'_{5y})+\cdots.\end{aligned} \quad (29)$$

Equation (29) describes the phase point part of the integral Eq. (15). To express the slope part of our algorithm, we apply the Taylor theorem to the slopes of Eq. (15) in the discrete geometry again:

$$S_{1x}=S_{2x}-hS'_{2x}+\frac{h^2}{2}S''_{2x}-\frac{h^3}{3!}S^{(3)}{}_{2x}+\cdots, \quad (30)$$

$$S_{1y}=S_{4y}-hS'_{4y}+\frac{h^2}{2}S''_{4y}-\frac{h^3}{3!}S^{(3)}{}_{4y}+\cdots, \quad (31)$$

$$S_{3x}=S_{2x}+hS'_{2x}+\frac{h^2}{2}S''_{2x}+\frac{h^3}{3!}S^{(3)}{}_{2x}+\cdots, \quad (32)$$

$$S_{3y}=S_{5y}-hS'_{5y}+\frac{h^2}{2}S''_{5y}-\frac{h^3}{3!}S^{(3)}{}_{5y}+\cdots, \quad (33)$$

$$S_{8y}=S_{5y}+hS'_{5y}+\frac{h^2}{2}S''_{5y}+\frac{h^3}{3!}S^{(3)}{}_{5y}+\cdots, \quad (34)$$

$$S_{6x}=S_{7x}-hS'_{7x}+\frac{h^2}{2}S''_{7x}-\frac{h^3}{3!}S^{(3)}{}_{7x}+\cdots, \quad (35)$$

$$S_{8x}=S_{7x}+hS'_{7x}+\frac{h^2}{2}S''_{7x}+\frac{h^3}{3!}S^{(3)}{}_{7x}+\cdots, \quad (36)$$

$$S_{6y}=S_{4y}+hS'_{4y}+\frac{h^2}{2}S''_{4y}+\frac{h^3}{3!}S^{(3)}{}_{4y}+\cdots, \quad (37)$$

$$S_{2y}=S_{7y}-2hS'_{7y}+2h^2S''_{7y}-\frac{4h^3}{3}S^{(3)}{}_{7y}+\cdots, \quad (38)$$

$$S_{7y}=S_{2y}+2hS'_{2y}+2h^2S''_{2y}+\frac{4h^3}{3}S^{(3)}{}_{2y}+\cdots, \quad (39)$$

$$S_{4x}=S_{5x}-2hS'_{5x}+2h^2S''_{5x}-\frac{4h^3}{3}S^{(3)}{}_{5x}+\cdots, \quad (40)$$

$$S_{5x}=S_{4x}+2hS'_{4x}+2h^2S''_{4x}+\frac{4h^3}{3}S^{(3)}{}_{4x}+\cdots. \quad (41)$$

Combining all of the equations above, we obtain

$$\begin{aligned}&\frac{h}{2}(2S_{5x}-2S_{4x}+2S_{7y}-2S_{2y}-S_{8x}\\&-S_{8y}+S_{1x}+S_{1y}-S_{3x}+S_{3y}+S_{6x}-S_{6y})\\&=h^2(S'_{4x}+S'_{5x}+S'_{2y}+S'_{7y}-S'_{2x}-S'_{4y}-S'_{7x}-S'_{5y})\\&-h^3(S''_{7y}-S''_{2y}+S''_{5x}-S''_{4x})+\cdots.\end{aligned} \quad (42)$$

Substituting Eq. (42) into Eq. (29) and reducing the expression gives

$$\begin{aligned}W=&\frac{(W_1+W_3+W_6+W_8)}{4}+\frac{h}{16}\\&\times(2S_{4x}-2S_{5x}+2S_{2y}-2S_{7y}-S_{8x}-S_{8y}\\&+S_{1x}+S_{1y}-S_{3x}+S_{3y}+S_{6x}-S_{6y})+\frac{1}{48}O(h^4)+\cdots.\end{aligned} \quad (43)$$

Eq. (43) is the expression for our phase-estimation equation with remaining error $\frac{1}{48}O(h^4)$. According to Pathak and Boruah [21], the truncation error in Southwell is $\frac{1}{12}O(h^4)$. Thus the error of the proposed algorithm is one-fourth of that in Southwell, for high-order aberrations.

## III. NUMERICAL SIMULATION RESULTS

This section focuses on comparisons between the proposed algorithm and those of Phuc, Pathak and Southwell in three aspects: reconstructing a wavefront aberration represented by Zernike polynomials, considering the convergence rates of each algorithm, and considering the influence of noise on the proposed method.

### 3.1. Algorithm Accuracy

Initially we use the Zernike polynomials, as numbered by Noll [22], as a sample set to describe the distorted wavefront. The higher order of this Zernike polynomial set means a higher order of optical aberrations [23]. In this simulation the first 36 Zernike terms are used in the reconstruction process, and a discretization domain of 300 × 300 sampling phase points is examined. For the $N \times N$ grid points, approximately $2N$ iterations are required for the SOR method to ensure good performance of the reconstruction operation, as reported by Southwell [11]. Therefore, our simulation used 1000 iterations for each of the algorithms considered here, to pursue good convergence. These results are illustrated in Fig. 3.

In this simulation, the relative root-mean-square error R is estimated to compare the accuracy of the algorithms. R can be defined as

$$\mathrm{R}=[\Delta W/W]^{1/2}, \quad (44)$$

where $W$ is the original wavefront and $\Delta W$ is the wavefront estimation error.

As shown in Fig. 3, the relative errors of the Southwell, Phuc and Pathak algorithm increase dramatically as the

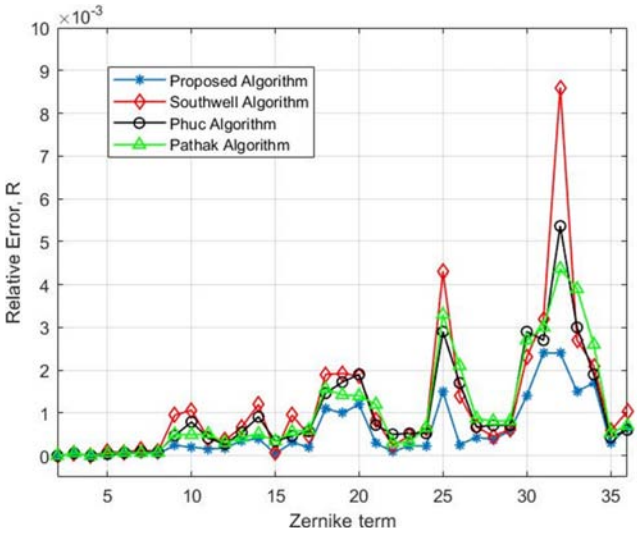


**FIG. 3.** Comparison of relative error levels of the algorithms. The simulated wavefront aberrations are Zernike polynomials, from 2nd term to 36th term.

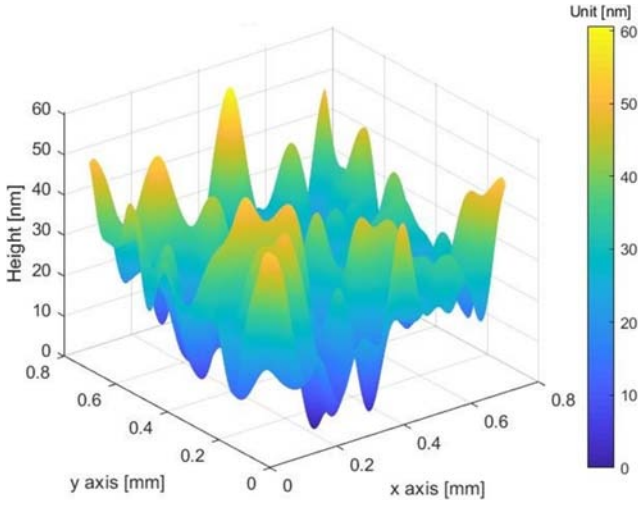


**FIG. 4.** The random Gaussian rough surface for the simulation.

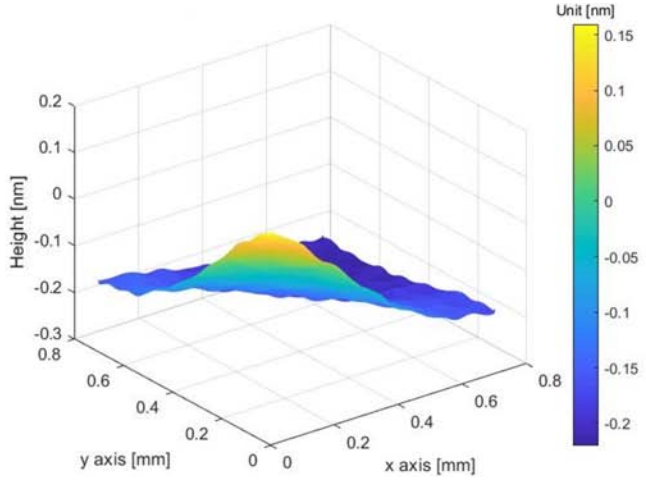


(a)

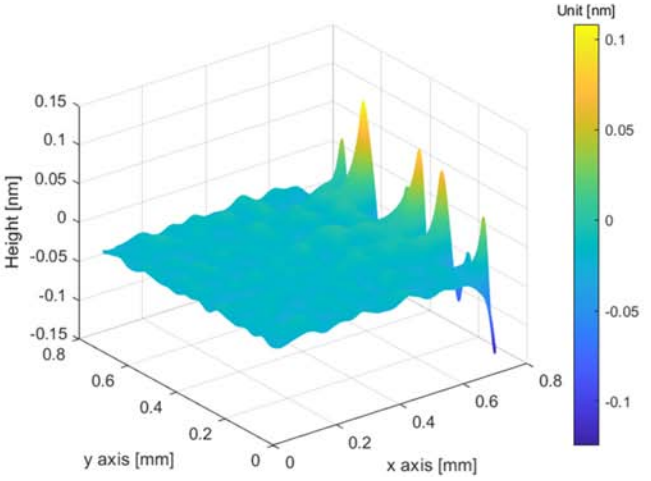


(b)

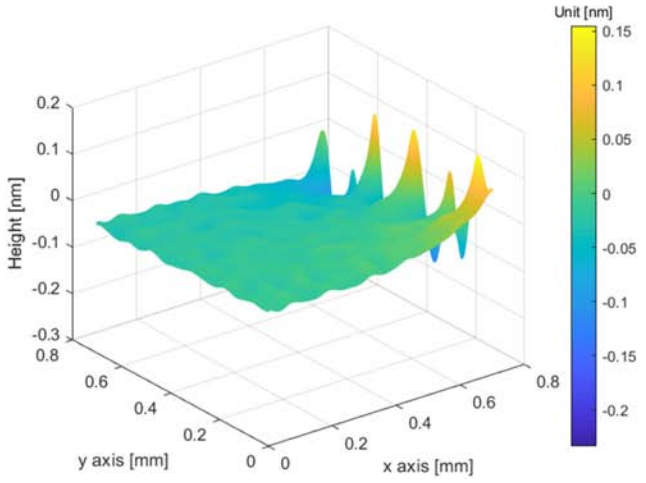


(c)

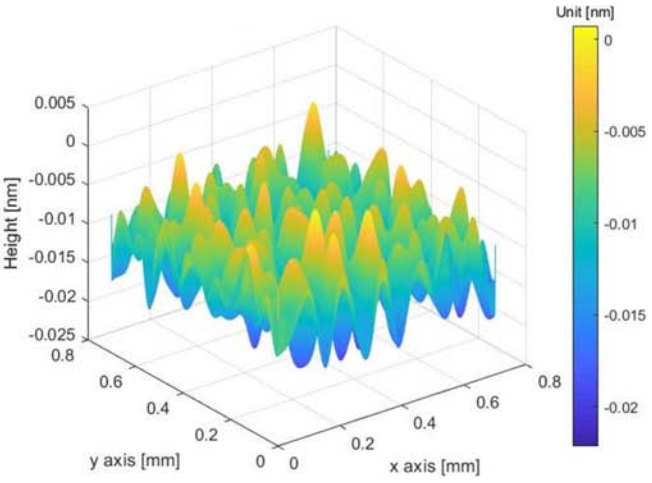


(d)

**FIG. 5.** Residual error between the ideal and the reconstructed surface, by (a) Southwell [11], (b) Phuc [18], (c) Pathak [17], and (d) proposed algorithms.

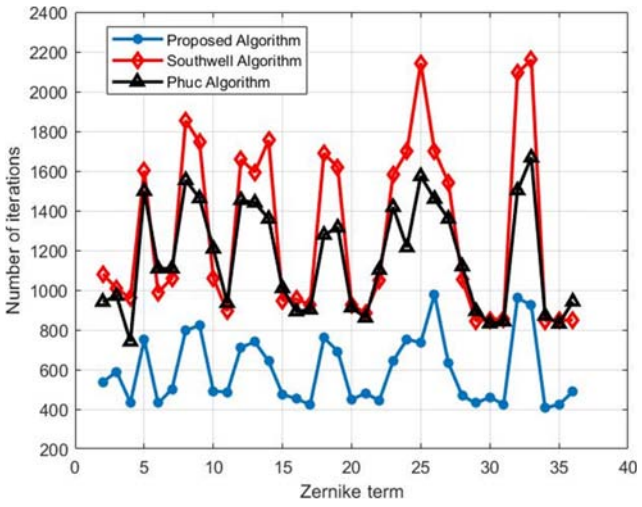


**FIG. 6.** Convergence rates of the algorithms for the first 36 Zernike terms.

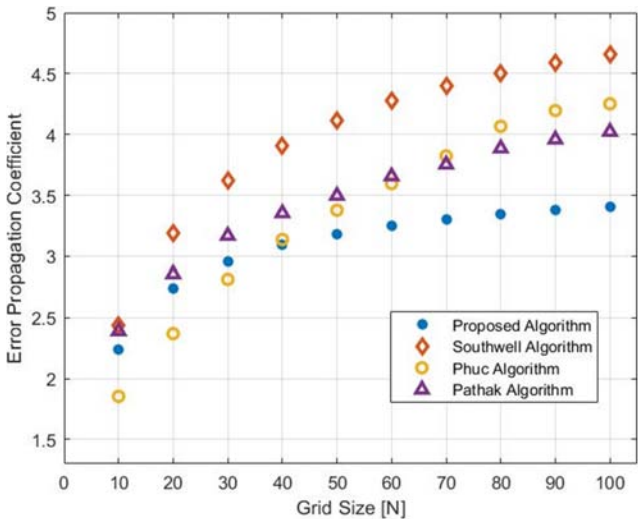


**FIG. 7.** Comparison of the error-propagation rates of four algorithms. *N* is the size of the grid in one dimension (that is, from 10 to 100).

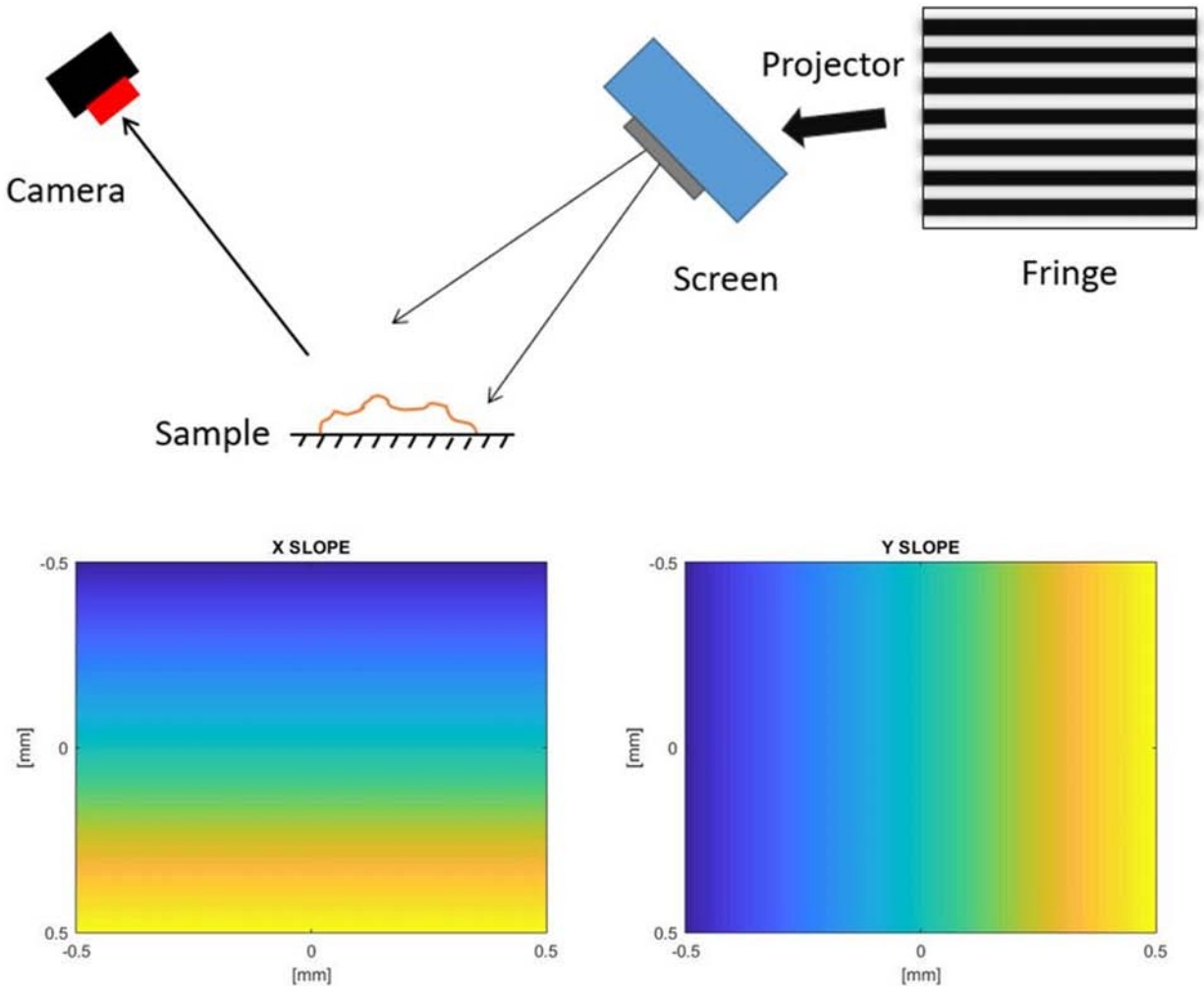


**FIG. 8.** Concept of defelectometry, and its output. The sinusoidal fringe patterns are projected onto the sample, and the slope data can be obtained from the image information taken by the camera.

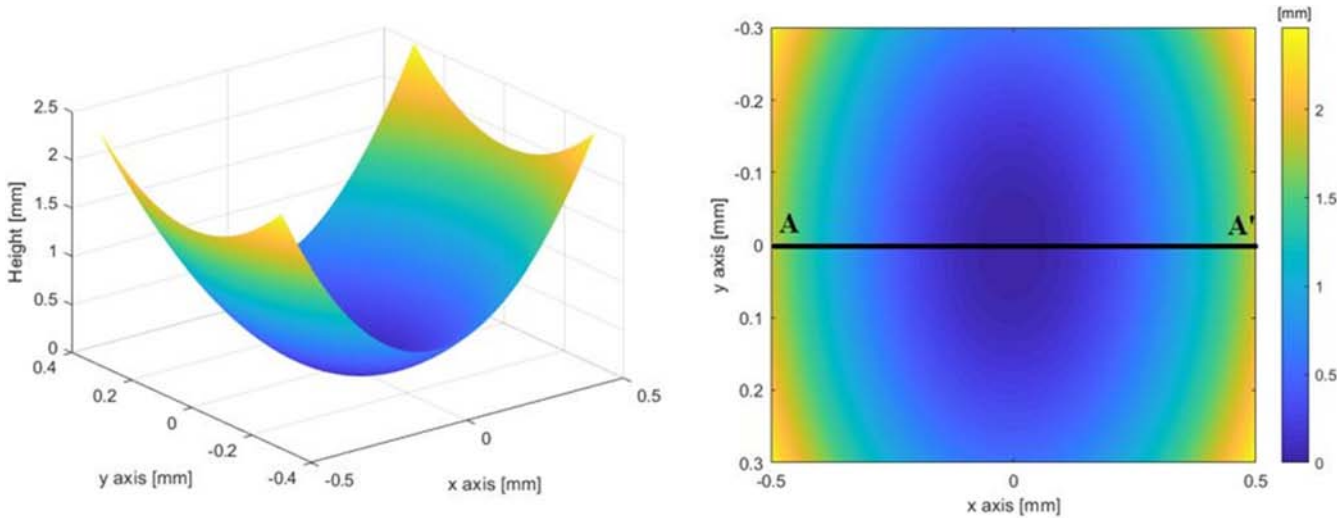


(a)

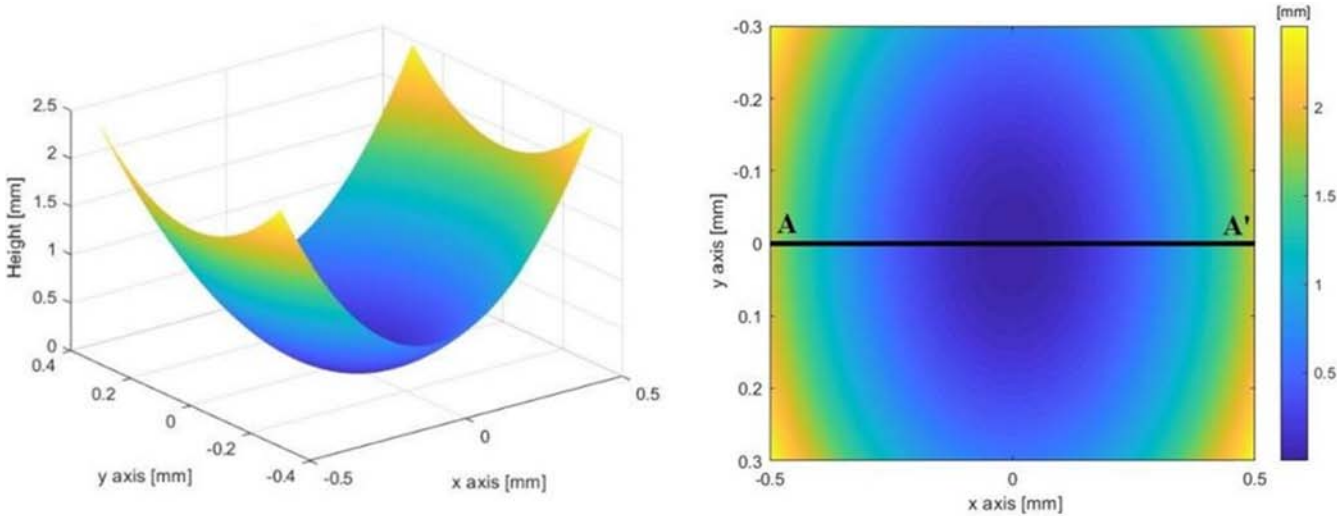


(b)

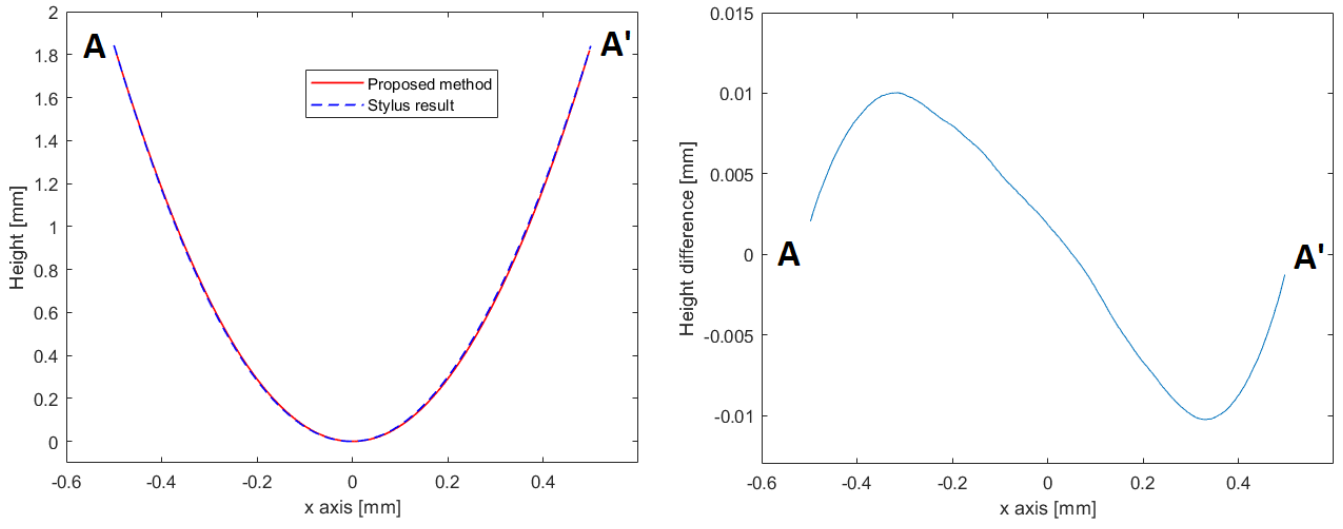


(c)

**FIG. 9.** 3D surface profile map: (a) reconstructed using the proposed method, (b) measured by a commercial stylus, and (c) comparison result of the A-A' line profiles by the two methods.

order of the Zernike terms increases. On the other hand, the error of the proposed algorithm does not exceed 0.003 for the first 36 Zernike terms.

For a very complicated surface, we select the rough surface shown in Fig. 4 as the original wavefront.

The simulation results are illustrated in Fig. 5: As shown, the reconstruction error of the proposed algorithm is minor, with a maximum of 0.02 nm.

### 3.2. Algorithm Speed

To evaluate the speed of the algorithm, we consider the convergence rate as a relative factor. In this section, we reconstruct the first 36 Zernike terms and stop the iterative loops when the relative error R is smaller than 0.001, or when it reaches its minimum value. This result is given in Fig. 6. Based on Fig. 6, it is clear that the convergence rate of the proposed method is greatly improved, compared to that for the Southwell and Phuc algorithms. Our algorithm only needs 400 to 500 iterations to converge (except for certain strange Zernike terms in each aberration order), while the Southwell and Phuc methods require approximately 1000 iterations to converge. In the case of Pathak's algorithm, more than 30,000 iterations are required to attain convergence.

### 3.3. Noise-propagation Analysis

To analyze the sensitivity of the reconstruction algorithm to noise, we use the error-propagation coefficient (EPC) introduced by Zou and Rolland [15]. This result is shown in Fig. 7.

The relative EPC is calculated following the incremental grid size of the wavefront. A smaller EPC implies that the algorithm is less sensitive to measurement noise. In Fig. 7, the proposed method has a smaller EPC value than that for the Southwell, Pathak, and Phuc methods. Thus the present approach offers better noise resistance.

## IV. EXPERIMENTAL IMPLEMENTATION

To verify the capabilities of our algorithm, a heads-up display (HUD) sample is measured by a deflectometry system, and the results compared to those for a reference obtained using a commercial stylus system. The concept of our deflectometry and the corresponding slope output are shown in Fig. 8.

The principle of a deflectometry system is such that sinusoidal fringe patterns along the horizontal and vertical directions are generated by a computer, shown on a screen, and projected onto the measurand. The images reflected from the surface of the target are then captured by a camera. Using supplementary information from a calibration process, we finally obtain the local slopes of the target surface [24], as shown in Fig. 8. Inputting these data into the proposed algorithm yields the reconstructed surface of our measurand, as illustrated in Fig. 9. Figures 9(a)–9(c) provide the reconstructed 3D shape of the HUD, and a comparison of our measured results to the profile surface produced by the stylus system. These two wavefront shapes and A-A' line profiles are very similar; the difference between them is less than 10 μm. The algorithms of Southwell, Phuc and Pathak also obtain similar results, but the maximum difference compared to the reference is around 20 μm, and it requires nearly 2,200 iterations to converge, whereas the proposed method only needs approximately 1,200 iterations.

## V. CONCLUSION AND DISCUSSION

The concept of a new integral equation to estimate phase by a zonal wavefront-reconstruction method was demonstrated in this paper. To obtain a more accurate estimation of phase error and convergence rate, especially for higher-order wavefront aberrations, we naturally incorporated a greater number of slopes in the proposed algorithm equation without increasing the spacing of the phase points. A mathematical description of the remaining error after using our method was also given, and compared to the results of the Southwell algorithm. Subsequently, numerical simulations and an experiment were conducted to verify the accuracy and speed of the proposed approach.

The simulation results in Figs. 3 and 6 demonstrated that there are several very strange Zernike terms in each order of the optical aberration. These Zernike terms had significant relative errors and required more iterations to reach convergence. In the future, we plan to devise a method that improves the reconstruction performance of these strange Zernike terms.

## FUNDING

This study was supported by the Commercialization Promotion Agency for R&D Outcomes (COMPA), "Real-time 3D surface measurement for aspheric and freeform lens", funded by the Ministry of Science and ICT(MSIT).

## REFERENCES

1. J. H. Lee, S. E. Lee, and Y. J. Kong, "Performance prediction of a laser-guide star adaptive optics system for a 1.6 m telescope," Curr. Opt. Photonics **2**, 269–279 (2018).
2. J. H. Lee, S. Shin, G. N. Park, H.-G. Rhee, and H.-S. Yang, "Atmospheric turbulence simulator for adaptive optics evaluation on an optical test bench," Curr. Opt. Photonics **1**, 107–112 (2017).
3. K. Ahn, S.-H. Lee, I.-K. Park, and H.-S. Yang, "Simulation of a laser tomography adaptive optics with Rayleigh laser guide stars for the satellite imaging system," Curr. Opt. Photonics **5**, 101–113 (2021).
4. Y.-S. Ghim, H.-G. Rhee, A. Davies, H.-S. Yang, and Y.-W. Lee, "3D surface mapping of freeform optics using wavelength scanning lateral shearing interferometry," Opt. Express **22**, 5098–5105 (2014).
5. M. T. Nguyen, Y.-S. Ghim, and H.-G. Rhee, "Single-shot de-

flectometry for dynamic 3D surface profile measurement by modified spatial-carrier frequency phase-shifting method," Sci. Rep. **9**, 3157 (2019).
6. M. P. Rimmer, "Method for evaluating lateral shearing interferograms," Appl. Opt. **13**, 623–629 (1974).
7. J. Herrmann, "Least-squares wave front errors of minimum norm," J. Opt. Soc. Am. **70**, 28–35 (1980).
8. E. P. Wallner, "Optimal wave-front correction using slope measurements," J. Opt. Soc. Am. **73**, 1771–1776 (1983).
9. L. Huang and A. Asundi, "Improvement of least-squares integration method with iterative compensations in fringe reflectometry," Appl. Opt. **51**, 7459–7465 (2012).
10. K. R. Freischlad and C. L. Koliopoulos, "Modal estimation of a wave front from difference measurements using the discrete Fourier transform," J. Opt. Soc. Am. A **3**, 1852–1861 (1986).
11. W. H. Southwell, "Wave-front estimation from wave-front slope measurements," J. Opt. Soc. Am. **70**, 998–1006 (1980).
12. R. Cubalchini, "Modal wave-front estimation from phase derivative measurements," J. Opt. Soc. Am. **69**, 972–977 (1979).
13. R. H. Hudgin, "Wave-front reconstruction for compensated imaging," J. Opt. Soc. Am. **67**, 375–378 (1977).
14. D. L. Fried, "Least-square fitting a wave-front distortion estimate to an array of phase-difference measurements," J. Opt. Soc. Am. **67**, 370–375 (1977).
15. W. Zou and J. P. Rolland, "Quantifications of error propagation in slope-based wavefront estimations," J. Opt. Soc. Am. A **23**, 2629–2638 (2006).
16. G. Li, Y. Li, K. Liu, X. Ma, and H. Wang, "Improving wavefront reconstruction accuracy by using integration equations with higher-order truncation errors in the Southwell geometry," J. Opt. Soc. Am. A **30**, 1448–1459 (2013).
17. B. Pathak and B. R. Boruah, "Improved wavefront reconstruction algorithm for Shack–Hartmann type wavefront sensors," J. Opt. **16**, 055403 (2014).
18. P. H. Phuc, N. T. Manh, H.-G. Rhee, Y.-S. Ghim, H.-S. Yang, and Y.-W. Lee, "Improved wavefront reconstruction algorithm from slope measurements," J. Korean Phys. Soc. **70**, 469–474 (2017).
19. Y. Saad and H. A. van der Vorst, "Iterative solution of linear systems in the 20th century," J. Comput. Appl. Math. **123**, 1–33 (2000).
20. C. Canuto and A. Tabacco, "Taylor expansions and applications BT," in *Mathematical Analysis I*, C. Canuto and A. Tabacco, Eds., 2nd ed. (Springer International Publishing, Charm, Germany. 2015), pp. 225–257.
21. B. Pathak and B. R. Boruah, "Improvement in error propagation in the Shack-Hartmann-type zonal wavefront sensors," J. Opt. Soc. Am. A **34**, 2194–2202 (2017).
22. R. J. Noll, "Zernike polynomials and atmospheric turbulence," J. Opt. Soc. Am. **66**, 207–211 (1976).
23. V. Lakshminarayanan and A. Fleck, "Zernike polynomials: a guide," J. Mod. Opt. **58**, 545–561 (2011).
24. M. T. Nguyen, P. Kang, Y.-S. Ghim, and H.-G. Rhee, "Nonlinearity response correction in phase-shifting deflectometry," Meas. Sci. Technol. **29**, 045012 (2018).